Solid Element Rotordynamic Modeling of a Rotor on a Flexible Support Structure Utilizing Multiple-Input and Multiple-Output Support Transfer Functions

Lingnan Hu[1]
Department of Mechanical Engineering,
Texas A&M University,
3123 TAMU,
College Station, TX 77843
e-mail: lingnan@tamu.edu

Alan Palazzolo
TEES Professor
Fellow ASME
Department of Mechanical Engineering,
Texas A&M University,
3123 TAMU,
College Station, TX 77843
e-mail: a-palazzolo@tamu.edu

The authors present an improved modeling approach to analyze the coupled rotor-support dynamics by modeling the rotor with solid finite elements (FEs) and utilizing multiple-input and multiple-output transfer functions (TFs) to represent the flexible support. A state-space model is then employed to perform general rotordynamic analyses. Transfer functions are used to simulate dynamic characteristics of the support structure, including cross-coupling between degrees-of-freedom. These TFs are derived by curve-fitting the frequency response functions of the support model at bearing locations. The impact of the polynomial degree of the TF on the response analysis is discussed, and a general rule is proposed to select an adequate polynomial degree. To validate the proposed approach, a comprehensive comparison between the complete solid FE rotor-support model (CSRSM) and the reduced state-space model (RSSM) is presented. Comparisons are made between natural frequencies, critical speeds, unbalance response, logarithmic decrement, and computation time. The results show that the RSSM provides a dynamically accurate approximation of the solid FE model in terms of rotordynamic analyses. Moreover, the computation time for the RSSM is reduced to less than 20% of the time required for the CSRSM. In addition, the modes up to 100,000 cpm are compared among the super-element, beam element, and RSSM. The results show that the RSSM is more accurate in predicting high-frequency modes than the other two approaches. Further, the proposed RSSM is useful for applications in vibration control and active magnetic bearing systems. [DOI: 10.1115/1.4034207]

Introduction

The beam-type FE method has been widely used to model common shafts and yields acceptable prediction results in most cases [1–5]. However, modern turbomachinery designs require lighter-weight, higher-speed rotor systems, which may require thin-walled rotors with thin disks operating at higher speeds on flexible supports. This is especially the case with aircraft gas turbine engines where low weight is a primary design goal. In addition, active magnetic bearing (AMB)-mounted machines require accurate prediction of the modes that are well above the operating speed to maintain stable levitation control. It is also recommended by API standards 617 for compressors [6] that the effects of the support structure should be considered in analysis of the unbalance response of the rotor system. One-dimensional (1D) beam-type FEs may be inadequate for modeling support structures with complex shapes and may also fail to provide accurate prediction of high-frequency modes when rotors become thin walled or when disk modes become important. Moreover, the isolated support impedance approaches may introduce errors if modeling support structures that have modes that are highly coupled between bearings and directions at the bearing locations.

An alternative approach is to utilize the solid FE method, which provides a flexible and accurate means for modeling coupled rotor-support dynamics. The 2D axisymmetric solid harmonic FE method [7–9], which accounts for the gyroscopic effects and the asymmetric and cross-coupled stiffness coefficients of the bearing, has been used to model rotating shafts and disks. For a short flexible rotor, in particular a thin-walled shaft with flexible disks, the axisymmetric solid FE model is more accurate in rotordynamics prediction than a beam FE model. Due to the dimensional limitations of the 1D and 2D FEs, the 3D solid elements are widely used to model complicated casing and support structures. Although it is viable to use a complete solid FE model including the rotor and support structures to perform rotordynamic analysis, especially at the design stage, it may require a large amount of computational resources and computation time. A remedy for this is to model the support structures with super-elements, which condense the internal degrees-of-freedom (DOFs) but retain the DOFs of the attachment nodes that connect the rotor and support substructures through the bearings [10].

In comparison with the solid FE and super-element models, an experimental approach is to obtain the frequency-dependent stiffness and damping of the support structure by measuring the frequency response functions (FRFs) at the bearings and then include the equivalent physical models of the structure in the analysis of the rotor system [11]. Vázquez and Barrett [12–14] extract a series of rational TFs from the measured FRFs of the support structure by using identification techniques. Both unbalance response and stability analyses of the rotor and support structure are accomplished with the TFs in the s-plane. Moore et al. [15] apply the 1D beam FE and 3D solid FE in modeling the rotor and housing of a large industrial turbocompressor, respectively, and develop point TFs to investigate the effects of the housing on the rotor system. In the work by De Santiago and Abraham [16], the power turbine

[1]Corresponding author.

Contributed by the Structures and Dynamics Committee of ASME for publication in the Journal of Engineering for Gas Turbines and Power. Manuscript received June 17, 2016; final manuscript received June 24, 2016; published online August 16, 2016. Editor: David Wisler.

that is commonly used in the oil and gas industries as a mechanical driver is modeled with solid elements, and the comparison with the complete rotor-support FE model shows that the simplified structure model utilizing the support TFs is applicable in the rotordynamic analysis.

This paper presents an alternative modeling approach for a complete rotor-support system, which takes advantage of both axisymmetric solid FE rotor model (accurate prediction of the dynamics of a rotor with complex shapes) and simplified support structure model utilizing the multiple-input and multiple-output (MIMO) support TFs (reduction of the computation time and requirement for computational resources). A thin-walled shaft with multiple flexible disks is modeled using the axisymmetric solid harmonic FE method. The flexible structure supporting the rotor is first modeled with solid elements, and then the bearing location FRFs are determined by calculating the corresponding receptances over the frequency range of interest. Subsequently, the corresponding FRFs of the support structure are obtained by using the curve-fitting technique [17]. Guidance is provided for selecting an adequate polynomial degree of the TFs of the support structure. The TFs representing the support structure are rearranged to constitute a TF matrix, which contains the necessary information for unbalance response and stability analysis of the entire rotor system. The TF matrix is further transformed into a state-space form. In general, however, the support TF model is MIMO, implying that the way of transforming the TF into the state-space form for a single-input and single-output (SISO) system [18] needs modifications. Finally, the state-space support model is connected with the rotor FE model by bearing forces.

The proposed RSSM that consists of a solid FE rotor model and a state-space support model is compared with the CSRSM. General rotordynamic analyses, such as natural frequencies, critical speeds, unbalance response, and logarithmic decrement (log dec), are compared in order to demonstrate the accuracy of using the RSSM in lieu of the CSRSM. In the meanwhile, the computation time is provided to show whether the proposed modeling approach is effective in model reduction. Furthermore, a thorough comparison of the rotor-support modes up to 100,000 cpm (~1667 Hz) is conducted among the RSSM, the solid FE rotor with a superelement support model (SRSSM), and the beam FE rotor with a solid FE support model (BRSSM).

Rotor Model

The solid model of an axisymmetric rotor can be reduced to a 2D plane (semisection of the rotor) model by using the axisymmetric harmonic FE method. As pointed out in Ref. [10], the 3D rotor may be formed in such a way that the displacements of the semisection plane are expanded circumferentially about the symmetric axis by following the Fourier series. The semisection area of the rotor, which is demonstrated in Fig. 1, is filled by triangular elements. The radial and axial displacements are correlated with the circumferential angle θ by

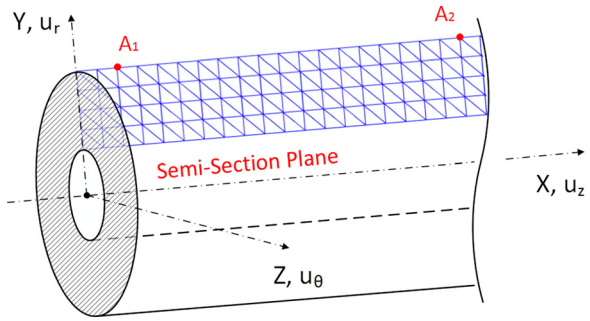

Fig. 1 Axisymmetric solid FE model of a hollow rotor

$$\begin{bmatrix} u_{mr} \\ u_{mz} \\ u_{m\theta} \end{bmatrix} = \begin{bmatrix} \sum_{i=1}^{3} N_{m,i} U_{mrS,i} \cos(m\theta) + \sum_{i=1}^{3} N_{m,i} U_{mrA,i} \sin(m\theta) \\ \sum_{i=1}^{3} N_{m,i} U_{mzS,i} \cos(m\theta) + \sum_{i=1}^{3} N_{m,i} U_{mzA,i} \sin(m\theta) \\ \sum_{i=1}^{3} N_{m,i} U_{m\theta S,i} \sin(m\theta) - \sum_{i=1}^{3} N_{m,i} U_{m\theta A,i} \cos(m\theta) \end{bmatrix} \tag{1}$$

where $N_{m,i}$ represents the shape functions of the three-node triangular element with the subscripts $i = 1, 2, 3$ indicating the three nodes. The harmonics $m = 0, 1$ are selected to account for gyroscopics and asymmetric and cross-coupled stiffness coefficients of the bearing. The resultant displacements of the rotor element in the radial, axial, and tangential directions, u_r, u_z and u_θ, are the sum of u_{mr}, u_{mz}, and $u_{m\theta}$, respectively, for all harmonics. The rotor FE model may be described by

$$[\mathbf{M}_R]\{\ddot{\mathbf{U}}_R\} + [\mathbf{G}_R]\{\dot{\mathbf{U}}_R\} + [\mathbf{K}_R]\{\mathbf{U}_R\} = \{\mathbf{f}_R\} \tag{2}$$

where $[\mathbf{G}_R]$ represents the gyroscopic matrix. The specific formulation of Eqs. (1) and (2) is provided in Ref. [9].

The Guyan reduction method [19] is used to reduce the rotor FE model and enhance the computational speed. Regarding the selection of retained DOFs for the Guyan reduction, a general rule is to retain the DOFs with large inertia, damping, or external load. The dynamic model described by Eq. (2) can then be rearranged to yield the following state-space form

$$\{\dot{\mathbf{q}}_R\} = [\mathbf{A}_R]\{\mathbf{q}_R\} + [\mathbf{B}_{RB}]\{\mathbf{f}_B\} + [\mathbf{B}_{RU}]\{\mathbf{f}_U\} \tag{3}$$

$$\{\mathbf{y}_R\} = [\mathbf{C}_R]\{\mathbf{q}_R\} \tag{4}$$

where $\{\mathbf{f}_B\}$ and $\{\mathbf{f}_U\}$ represent the bearing force vector and unbalanced force vector (any external load including unbalanced force), respectively. $\{\mathbf{q}_R\}$ is the state variable vector, and $\{\mathbf{y}_R\}$ are the displacements of the rotor at the bearing attachment points. All matrices and vectors in Eqs. (3) and (4) are given in the Appendix.

Support Structure Model

The support structure including the bearing pedestal is first modeled with solid tetrahedron elements. Then, the fictitious node, which corresponds to the attachment point of each bearing, is created to connect the rotor and support structure. As can be seen from Fig. 2, each fictitious node is connected by the rigid and

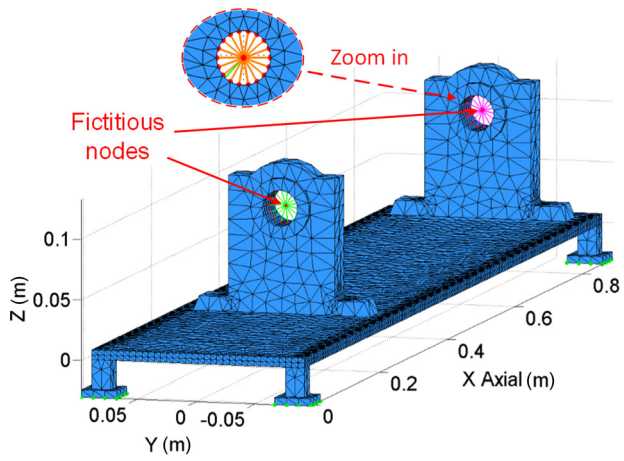

Fig. 2 Solid tetrahedron element mesh model of the support structure with two fictitious nodes

massless beams (a fictitious beam web) with the nodes that are circumferentially around the bearing center. In calculation, these rigid beams can be treated as the ones with the stiffness coefficients that are much higher than the modulus of elasticity of the support structure. The dynamics of the support FE model may be written as

$$[\mathbf{M}_S]\{\ddot{\mathbf{U}}_S\} + [\mathbf{C}_S]\{\dot{\mathbf{U}}_S\} + [\mathbf{K}_S]\{\mathbf{U}_S\} = \{\mathbf{f}_S\} \tag{5}$$

where $[\mathbf{C}_S]$ denotes the proportional damping matrix of the support structure.

Concerning the type of solid elements, the model with the hexahedron elements normally has a smaller size than that with the tetrahedron elements, thereby requiring less computation time. However, this may not be true if the shape of support structure is complex or the time for meshing is counted in the total simulation time, in which case it usually takes more time to generate the hexahedral mesh than the tetrahedral mesh, particularly at the boundaries. Hence, the influences of the solid element types are not quantified in the present paper.

The FRFs are obtained by using the support FE model instead of experimental measurement. First of all, we apply a virtual point force (in a sinusoidal form) at one fictitious node, which is representative of the bearing center. Then Eq. (5) is solved for forced responses at all bearing locations and in all directions. Take the support model shown in Fig. 2, for instance. One point force, F, is acted at one bearing location in one direction (indicated by the subscript Y or Z) and yields four responses, U_{Y_1}, U_{Z_1}, U_{Y_2}, and U_{Z_2} (one response for one bearing location and one direction). The responses can be finally correlated with the forces by the following equation:

$$\begin{bmatrix} U_{Y1} \\ U_{Z1} \\ U_{Y2} \\ U_{Z2} \end{bmatrix} = \begin{bmatrix} G_{Y1Y1} & G_{Y1Z1} & G_{Y1Y2} & G_{Y1Z2} \\ G_{Z1Y1} & G_{Z1Z1} & G_{Z1Y2} & G_{Z1Z2} \\ G_{Y2Y1} & G_{Y2Z1} & G_{Y2Y2} & G_{Y2Z2} \\ G_{Z2Y1} & G_{Z2Z1} & G_{Z2Y2} & G_{Z2Z2} \end{bmatrix} \cdot \begin{bmatrix} F_{Y1} \\ F_{Z1} \\ F_{Y2} \\ F_{Z2} \end{bmatrix} \tag{6}$$

where G is the FRF, and the subscripts 1 and 2 represent the first (left) and second (right) bearing locations shown in Fig. 2, respectively.

By utilizing the complex curve-fitting algorithm [17], we are able to obtain from the FRFs the rational TF that corresponds to the location and direction of each force-response pair. The optimal polynomial coefficients of the TF are obtained by minimizing the weighted sum of the squares of the amplitude errors between the frequency-dependent functions and polynomial ratios. The minimization of the errors depends on both sampling quality and polynomial degree of the TF. Two guidelines for acquiring an effective set of sampling frequencies are provided. The first is that the number of excitation frequencies should be sufficient to retain the dynamic information (amplitudes and phases) of the response in the neighborhood of the frequencies with a dramatic amplitude or phase change. Second, the final frequency sample should be the union of the frequencies of all the sixteen FRFs. A general rule for the selection of the polynomial degree is to ensure that the curve fit retains the peaks and shifts of the TF amplitude or phase while avoiding a higher polynomial degree than needed. This is because high-degree polynomials can be highly oscillatory, which may include undesired information, such as noises in modal testing. The derived TFs in the s-plane may be expressed as

$$G_{AiBj}(s) = \frac{b_1 s^m + b_2 s^{m-1} + \cdots + b_{m+1}}{s^n + a_1 s^{n-1} + \cdots + a_n} \tag{7}$$

where the subscripts A, B indicate Y or Z, and $i, j = 1$ or 2. For simplicity, the TF matrix in Eq. (6) is written as $[\mathbf{G}(s)]$.

It can be clearly seen that $[\mathbf{G}(s)]$ is a MIMO system. We may derive each SISO state space from the individual TF, $G_{AiBj}(s)$, and stack the state-space matrix into the corresponding block of the MIMO state space. There is the possibility that the final MIMO system is not a minimal state-space realization, leading to extra states and eigensolutions. Several theoretical approaches [20–22] may help to resolve this problem. A practical approach is to identify repeated modes by inspection of the mode shapes and frequencies. The final state-space support model can be expressed as

$$\{\dot{\mathbf{q}}_S\} = [\mathbf{A}_S]\{\mathbf{q}_S\} + [\mathbf{B}_S]\{\mathbf{f}_S\} \tag{8}$$

$$\{\mathbf{y}_S\} = [\mathbf{C}_S]\{\mathbf{q}_S\} \tag{9}$$

where $\{\mathbf{f}_S\}$ is the bearing force vector, $\{\mathbf{y}_S\}$ are the displacements of the support at the bearing attachment points. $[\mathbf{A}_S]$, $[\mathbf{B}_S]$, and $[\mathbf{C}_S]$ represent the system matrix, input matrix, and output matrix, respectively, and these three matrices can be obtained by transforming $[\mathbf{G}(s)]$ into a state-space form. The detailed composition of these matrices is given in the Appendix. $\{\mathbf{q}_S\}$ is the state variable vector that consists of purely mathematical variables without physical meanings. It can be seen from the Eqs. (8) and (9) that the support model is substantially reduced by utilizing the TFs and state-space model as the number of state variables is considerably smaller than the DOF number of the support structure.

System (State Space) Model

The rotor and support structure are connected by bearings, or more precisely, by bearing forces. The different forms of bearing forces that are written in Eqs. (3) and (8) can be correlated by

$$\{\mathbf{f}_S\} = -\{\mathbf{f}_B\} \tag{10}$$

With regard to most of the fluid film bearings, the bearing forces at a certain rotating speed may be applied to the rotor in the form of

$$F_B = c_B \cdot \dot{U}_B + k_B \cdot U_B \tag{11}$$

where U_B is the relative displacement between the rotor and support structure. Therefore, the general bearing forces can be derived from

$$\{\mathbf{f}_B\} = -[\mathbf{C}_B](\{\dot{\mathbf{y}}_R\} - \{\dot{\mathbf{y}}_S\}) - [\mathbf{K}_B](\{\mathbf{y}_R\} - \{\mathbf{y}_S\}) \tag{12}$$

Substituting Eqs. (10) and (12) into Eqs. (3), (4), (8), and (9) yields

$$[\mathbf{A}_T]\{\dot{\mathbf{q}}\} = [\mathbf{B}_T]\{\mathbf{q}\} + [\mathbf{B}_{UT}]\{\mathbf{f}_U\} \tag{13}$$

With Eq. (13) representing the entire state-space model of the rotor-support system, stability analysis of the system can be conducted by using the characteristic equation

$$\phi(s) = |s[\mathbf{I}] - [\mathbf{A}_T]| = 0 \tag{14}$$

If there are positive real eigenvalues or negative log dec, the rotor system is unstable. Additionally, unbalance response of the rotor can be obtained by substituting $\{\hat{f}_U\}e^{j\omega t}$ for $\{f_U\}$ into Eq. (13), which yields

$$(j\omega[\mathbf{A}_T] - [\mathbf{B}_T])\{\hat{\mathbf{q}}\} = [\mathbf{B}_{UT}]\{\hat{\mathbf{f}}_U\} \tag{15}$$

where $\{\hat{\mathbf{q}}\}$ represents the complex state vector in the state-space model, $\{\hat{\mathbf{f}}_U\}$ is the complex unbalanced force vector, and ω is the frequency of the unbalanced force.

Validation

To validate the modeling approach proposed in this paper, a scaled-down rotor-support system, which is modeled with either

the solid elements or both solid elements and TFs, is presented for investigation and comparison. The rotor consists of a thin-walled shaft and three disks and is supported by two tilting pad bearings. The axisymmetric harmonic FE method is used to model the thin-walled rotor, which is depicted in Fig. 3. The material properties of the rotor are set as $\rho = 7800\,\mathrm{kg/m^3}$, $\nu = 0.3$, $E = 2.1 \times 10^{11}\,\mathrm{N/m^2}$. The stiffness and damping of the bearings are obtained from a specialized bearing coefficient-prediction program and are given in Figs. 4 and 5. The structure supporting the rotor is composed of a bearing pedestal and a baseplate with four feet fixed to ground. The material properties of the support structure are given as $\rho = 2700\,\mathrm{kg/m^3}$, $\nu = 0.33$, $E = 6.9 \times 10^{10}\,\mathrm{N/m^2}$. Tetrahedron elements are used to model the support structure. The CSRSM is demonstrated in Fig. 6.

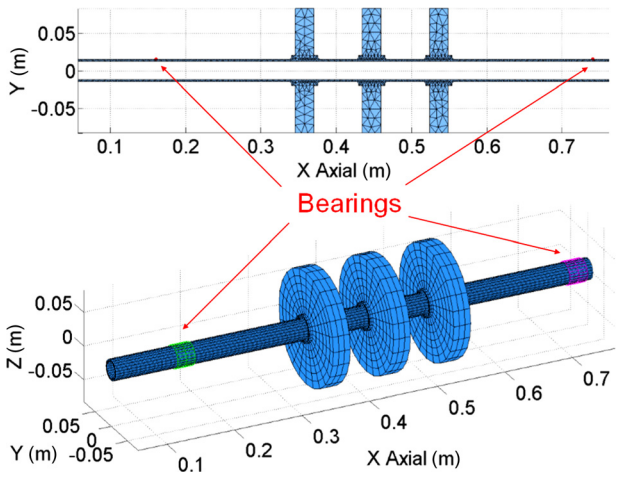

Fig. 3 Cross section (top) and 3D solid (bottom) FE mesh models of the rotor supported by two tilting-pad bearings

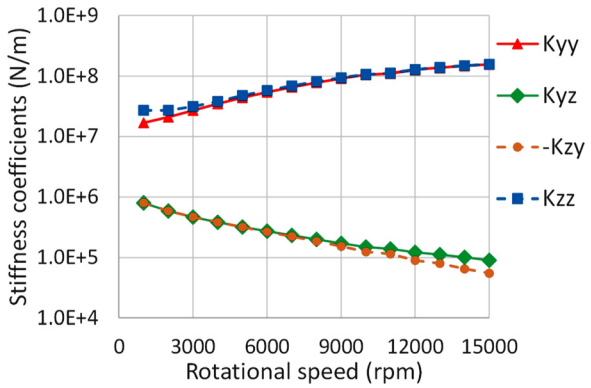

Fig. 4 Stiffness coefficients of the bearing

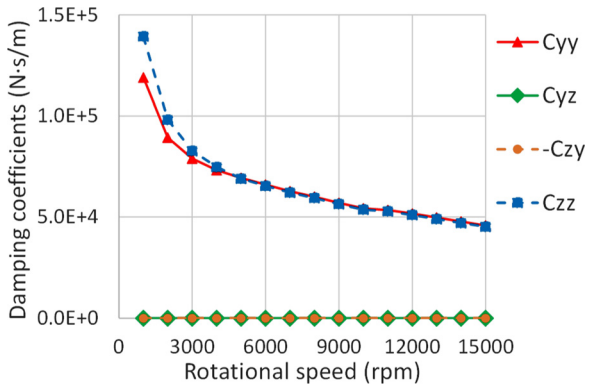

Fig. 5 Damping coefficients of the bearing

Grid Sensitivity and Curve-Fitting. Before the FE simulation results can be used for comparison, a grid sensitivity test on the CSRSM is conducted in order to validate the solid FE modeling. The damped natural frequencies of the third mode of the rotor-support system are calculated for comparison and are presented in Fig. 7. It can be seen that the percentage difference of the natural frequencies, compared to the natural frequencies obtained from the finest mesh, varies from 36.3% to 1.2%, which indicates that the natural frequencies converge with the refinement of mesh of the rotor and support. Therefore, the FE model with a 1.2% difference can be used as a benchmark in evaluation of the proposed modeling approach.

The FRF data are obtained by applying frequency-dependent load (sinusoidal forces) on the fictitious bearing attachment points of the support FE model. The TFs are subsequently obtained by curve-fitting these FRF data with polynomials, where extra attention needs be given to the polynomial order selection. Consider the curve-fitting with the lower degree TFs like the second-order numerator divided by third-order denominator (second/third) polynomials. It is found that not all the sixteen TFs in Eq. (6) are well fitted. Take G_{Z2Z2}, for example. The curve fit shown in Fig. 8 fails to capture the exact frequency (150 Hz) of the amplitude peak, where the rotor and support structure vibrate vertically (refer to the bottom figure shown in Fig. 11). Since G_{Z2Z2} represents the TF between the excitation force and response in the vertical direction at the right bearing location, the shifting of the critical frequency of G_{Z2Z2} probably leads to shifted vibration peaks or extra peaks. In order to solve this problem, a higher

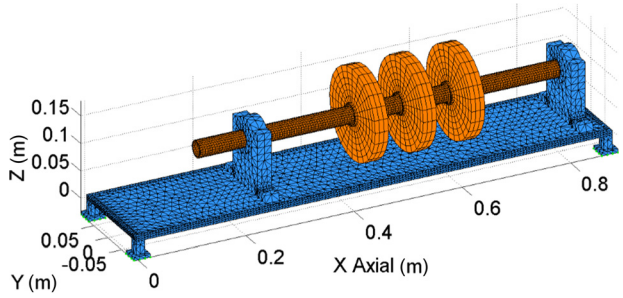

Fig. 6 Solid FE mesh model of the rotor-support system

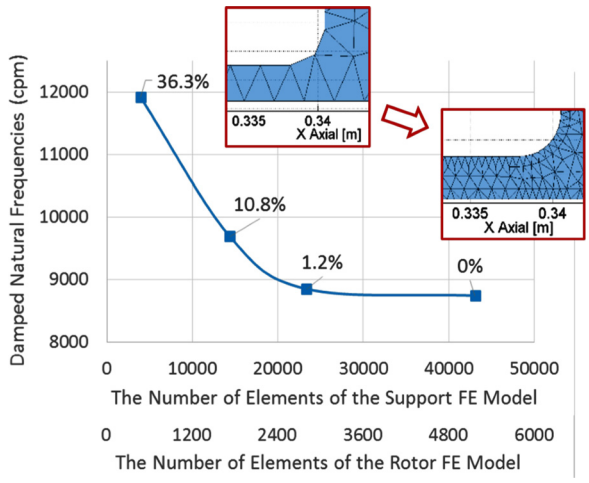

Fig. 7 Grid sensitivity test for the third mode of the CSRSM at the rotational speed of 5000 rpm

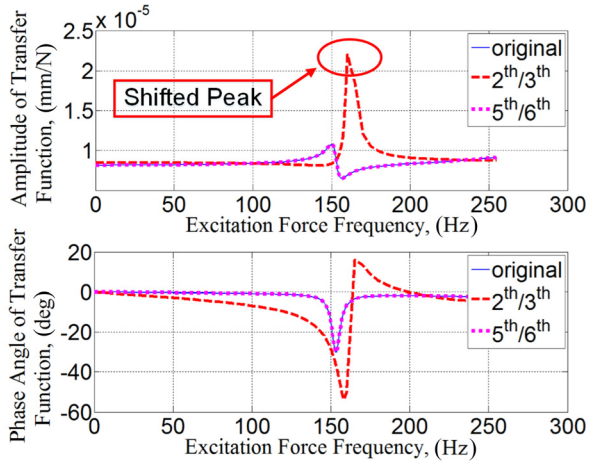

Fig. 8 Transfer function G_{Z2Z2} with the second/third and fifth/sixth polynomials

polynomial degree (fifth/sixth) is employed. As Fig. 8 shows, the fifth/sixth TF perfectly fits the original FRF curve.

For simplicity, the detailed TF matrices are not provided. After converting the TF matrices into a state space, the matrix formulas provided in the preceding sections are employed to combine the state-space model of the support structure with the rotor FE model.

Comparison of Rotordynamic Analyses. Simulation results of commonly applied rotordynamic analyses, such as the critical speed map, unbalance response, and log dec, are presented in Figs. 9–19.

In regard to the rotor-support system, the first four critical speeds to appear within the rotating speed range of 0–15,000 rpm are presented in Figs. 9 and 10, with the corresponding mode shapes shown in Figs. 11 and 12. As can be seen from Fig. 9, the first critical speed is 3140 rpm for the CSRSM and 3125 rpm for the RSSM. That is to say, the percentage difference of the first critical speeds between these two models is less than 0.5%. The second and fourth critical speeds obtained from the proposed RSSM are 3455 rpm and 13,769 rpm, respectively. For the CSRSM, they are 3455 rpm and 13,771 rpm, respectively. As demonstrated in Figs. 9 and 10, the natural frequency lines for these two modes nearly coincide with each other. The third critical speed of the RSSM is 8748 rpm with a 0.6% difference from 8805 rpm of the CSRSM. The close agreement confirms the accuracy of the proposed modeling approach compared with the complete solid FE modeling approach, in terms of the natural frequency prediction.

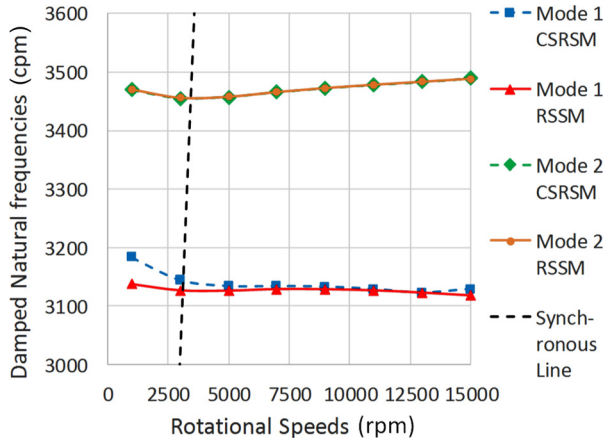

Fig. 9 Critical speeds for the first and second modes

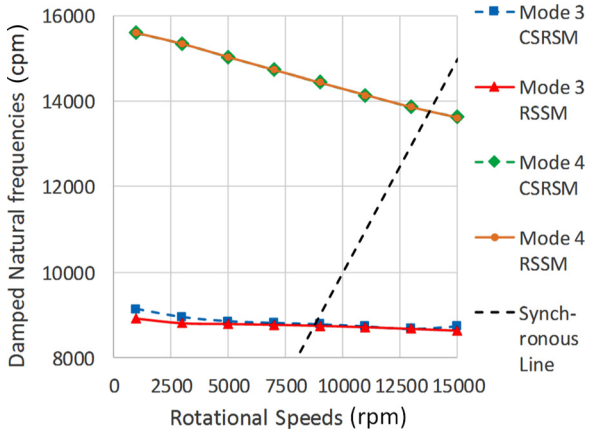

Fig. 10 Critical speeds for the third and fourth modes

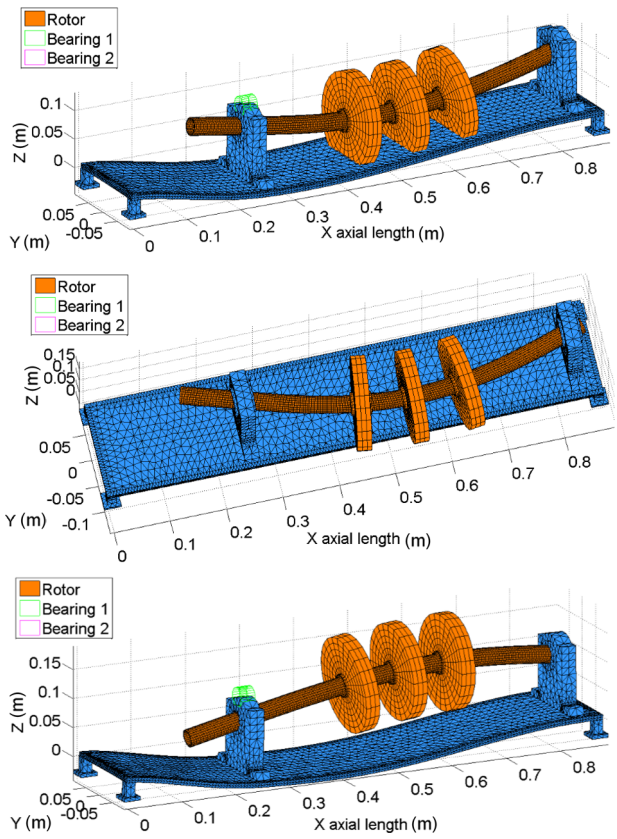

Fig. 11 Mode shapes for the first (top), second (middle), and third (bottom) critical speeds of the rotor-support system

To further validate the RSSM, unbalance response analysis is performed. The unbalanced mass distance of 25 g · mm is attached to the center of the middle disk. The peak-to-peak (p-p) unbalance response of the rotor at the middle disk and two bearing locations is demonstrated in Figs. 13–18. It can be clearly observed that the vibration amplitudes of the RSSM agree with those of the CSRSM. The highest vibration peaks at each of those three locations all occur at the speed of 3125 rpm (the first critical speed) or 3450 rpm (near the second critical speed). At the speed of 8830 rpm (close to the third critical speed), violent vibrations appear in the vertical direction, whereas the horizontal vibrations are much milder. This may be attributed to the mode coupling in

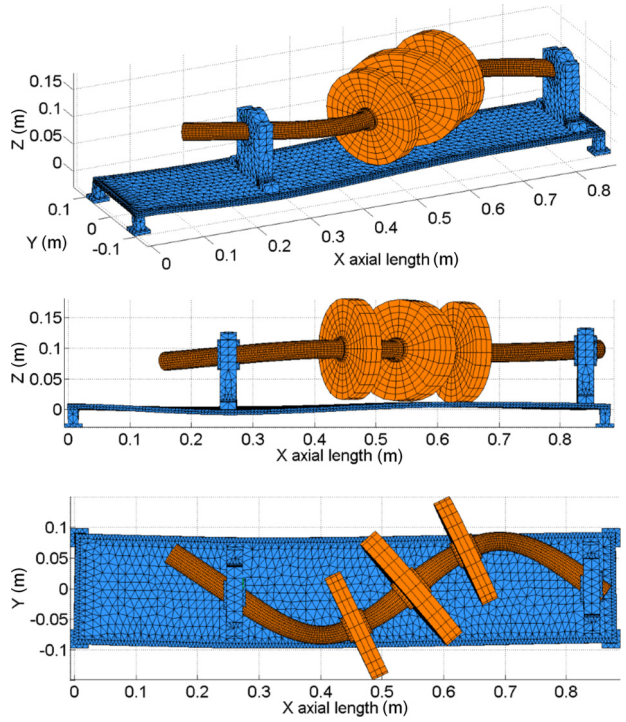

Fig. 12 Mode shape (top: orthographic projection, middle: front view, bottom: top view) for the fourth critical speed of the rotor-support system

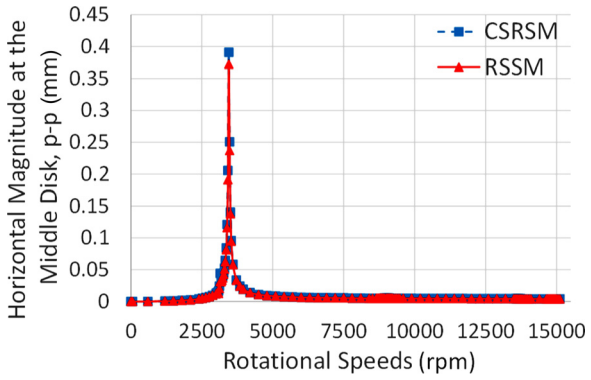

Fig. 13 Horizontal magnitude of the unbalance response at the center of the middle disk

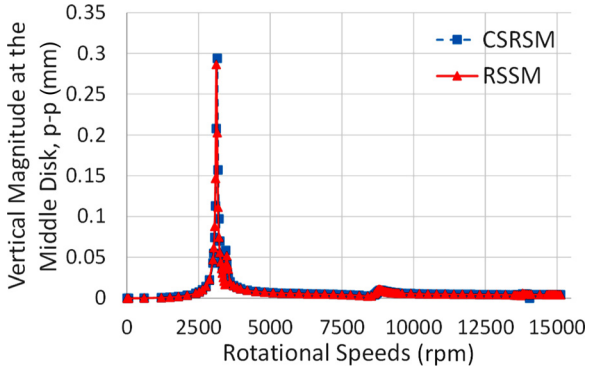

Fig. 14 Vertical magnitude of the unbalance response at the center of the middle disk

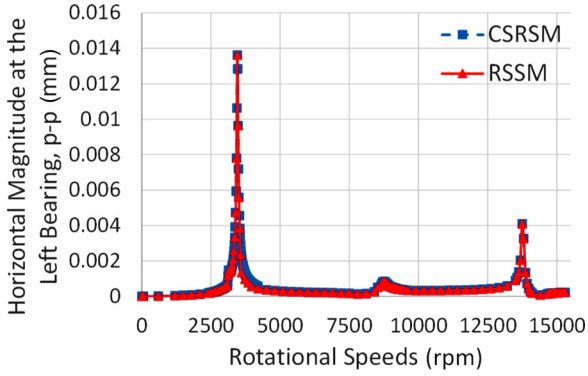

Fig. 15 Horizontal magnitude of the unbalance response at the left bearing location

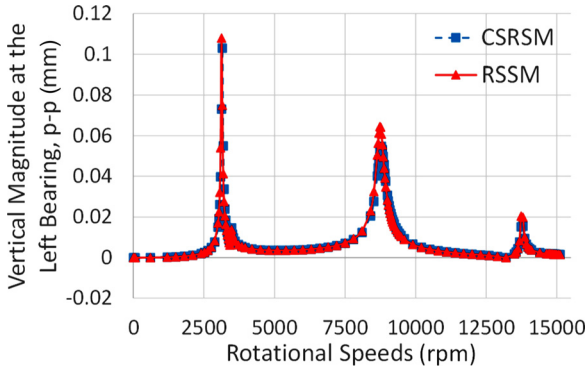

Fig. 16 Vertical magnitude of the unbalance response at the left bearing location

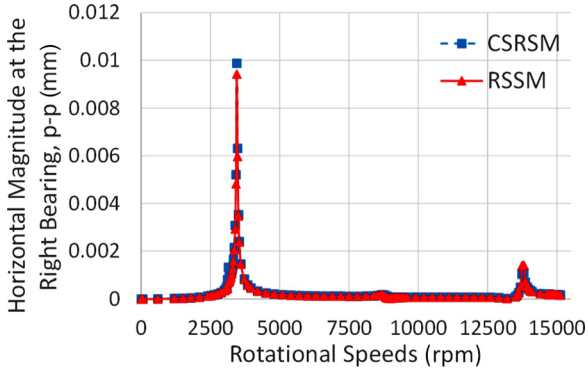

Fig. 17 Horizontal magnitude of the unbalance response at the right bearing location

the vertical direction between the rotor and support structure, as can be seen from the bottom mode shape depicted in Fig. 11. At 13,800 rpm (near the fourth critical speed), however, vibrations peak in both vertical and horizontal directions. This can be explained by the mode shapes shown in Fig. 12, where the rotor and support structure are not only coupled in the vertical direction but in horizontal direction as well, thereby leading to both vertical and horizontal vibration peaks.

Apart from the unbalance analysis, stability of the rotor system is always one of the primary concerns in rotordynamic analyses. The log dec of the rotor system, which is commonly used in the turbomachinery industry to determine the dynamic stability, is calculated and compared in Fig. 19. For the first, third, and fourth modes, the percentage difference of the log dec between the

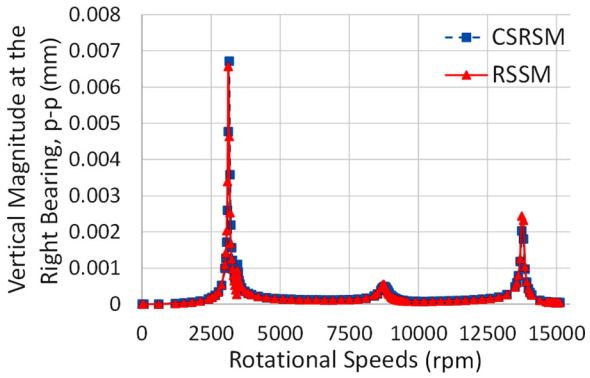

Fig. 18 Vertical magnitude of the unbalance response at the right bearing location

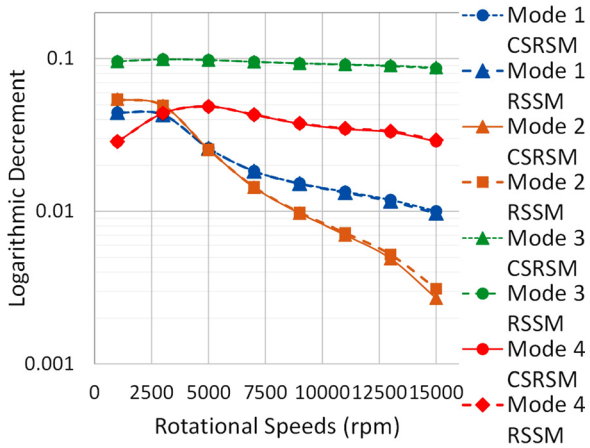

Fig. 19 Stability analysis of the rotor-support system

RSSM and the CSRSM is within 3%. With regard to the second mode within the operating speed range, the largest difference is 15%, which occurs at the speed of 15,000 rpm. In general, the RSSM shows good agreement with the CSRSM.

Comparison of Computation Time. In order to demonstrate the computational efficiency of the proposed approach, the computation time is compared among the CSRSM, RSSM, SRSSM, and BRSSM. Before comparison, the Guyan reduction method is applied to all the FE models, retaining 10% DOFs of each model. The comparison, as illustrated in Table 1, is made between the simulation time required for obtaining the eigenvalues of the lowest 100 modes of the rotor-support system. The simulation is performed on the HP Z420 workstation with a 3.7 GHz Quad-core Intel Xeon CPU and 48 GB RAM.

For the CSRSM, it takes 14 min to obtain the eigenvalues at each rotational speed. In contrast, the RSSM requires only 2.5 min. The reduction of the computation time benefits from the substantial reduction of the solid FE support structure model from 2537 DOFs to the 96×96 (96 DOFs) state-space model that corresponds to the fifth/sixth TFs of the support structure. Generally, rotordynamic analyses will be conducted at dozens of different rotational speeds, due to the gyroscopic effects, the change of the bearing or seal coefficients, etc. Also, both the mesh generation and the calculation of the FRFs are performed only once. Therefore, by counting the total simulation time, the RSSM is nearly five times faster than the CSRSM. This time reduction factor will increase with less DOFs of the rotor model and more DOFs of the support structure model as the RSSM mainly retains the DOFs of the rotor model.

In addition to the comparison with the solid FE model, the RSSM is compared with the SRSSM and BRSSM. As Table 1 shows, the computation time is 2.5 min for the RSSM versus 3 min for the BRSSM. This can be explained by the larger total number of DOFs of the BRSSM, i.e., the sum of DOFs of the beam FE rotor model (38 DOFs) and the solid FE support structure model (2537 DOFs) is more than the DOFs of the RSSM (2146 DOFs in total). In regard to the SRSSM, the reduced substructure (support structure) is assembled together with the rotor FE model via two bearing attachment points that are exterior to the super-element support model.

As illustrated in Table 1, either the computation time or the time for mesh generation is quite close between the RSSM and the SRSSM. Although the state-space support model seems to have many more DOFs (96 DOFs) than the super-element support model (6 DOFs), the computation difference between these two models is in practice less than three seconds on account of having nearly the same total number of DOFs (2146 DOFs versus 2056 DOFs).

Comparison of Higher-Frequency Mode Predictions. In contrast with the slight advantage of the SRSSM in computation time, the predictions made by the SRSSM are probably less accurate than the RSSM for some higher-frequency modes. To prove this, both the RSSM and the SRSSM are compared with the CSRSM in terms of natural frequencies. The BRSSM is also included in this comparison in order to show that the proposed modeling approach is more accurate than the beam rotor model in higher-frequency modes.

For the rotor-support system with the rotor spinning at 10,000 rpm, the natural frequencies of the modes up to 100,000 cpm (~1667 Hz) are given in Table 2. It can be seen that nearly all the natural frequencies of the RSSM are in close agreement with those of the CSRSM.

As for the SRSSM, most of the modes are in accordance with those of the CSRSM, except that modes 7 and 13 are inaccurately predicted (64% and 32% differences, respectively) and modes 15, 16, 17, and 20 are missing. The reason for these inaccurate or missing modes can be found in Fig. 20. As the top figure shows, the rotor and support are coupled in mode 7. It is likely that the support structure is over-reduced by using the super-element. As a result, the dynamic characteristics of the support structure modes that have a complex mode shape like mode 7 may not be perfectly represented by the support super-element model. In addition, the super-element support model fails to predict some of the

Table 1 Simulation time for obtaining the eigenvalues of the lowest 100 modes of the rotor-support system with 10% DOFs retained

	CSRSM	RSSM	SRSSM	BRSSM
Rotor model	2050 DOFs	2050 DOFs	2050 DOFs	38 DOFs
Support model	2537 DOFs	96×96 state-space matrix (96 DOFs)	6 DOFs	2537 DOFs
Total DOFs	4587	2146	2056	2575
Time for meshing	2 min	2 min	2 min	1.5 min
Computation time per speed	14 min	2.5 min	2.5 min	3 min
Time for obtaining FRFs		5 min		

Table 2 Natural frequencies of the rotor-support system at the rotational speed of 10,000 rpm

Natural frequency (cpm)	CSRSM	RSSM	SRSSM	BRSSM
Mode 1	3091	3086 (0%)	3092 (0%)	3171 (3%)
Mode 2	3485	3485 (0%)	3490 (0%)	3586 (3%)
Mode 3	8719	8705 (0%)	8868 (2%)	8809 (1%)
Mode 4	14,323	14,315 (0%)	14,509 (1%)	14,660 (2%)
Mode 5	17,471	17,451 (0%)	17,818 (2%)	17,748 (2%)
Mode 6	19,081	19,081 (0%)	19,081 (0%)	19,484 (2%)
Mode 7	21,615	21,430 (−1%)	35,391 (64%)	21,672 (0%)
Mode 8	29,588	29,584 (0%)	29,609 (0%)	31,137 (5%)
Mode 9	33,037	33,037 (0%)	33,037 (0%)	33,812 (2%)
Mode 10	37,350	36,986 (−1%)	40,213 (8%)	37,615 (1%)
Mode 11	41,473	41,422 (0%)	41,836 (1%)	42,621 (3%)
Mode 12	42,392	42,407 (0%)	42,554 (0%)	47,608 (12%)
Mode 13	47,938	49,359 (3%)	63,414 (32%)	47,960 (0%)
Mode 14	60,550	60,560 (0%)	60,549 (0%)	67,418 (11%)
Mode 15	64,606	67,945 (5%)	N/A	64,717 (0%)
Mode 16	70,190	67,914 (−3%)	N/A	70,224 (0%)
Mode 17	76,890	90,004 (17%)	N/A	76,892 (0%)
Mode 18	78,786	79,436 (1%)	93,125 (18%)	80,184 (2%)
Mode 19	85,458	85,458 (0%)	85,457 (0%)	95,523 (12%)
Mode 20	89,814	106,427 (18%)	N/A	104,394 (16%)
Mode 21	89,923	90,772 (1%)	91,865 (2%)	88,171 (−2%)
Mode 22	91,451	91,395 (0%)	91,349 (0%)	97,181 (6%)
Mode 23	98,168	98,495 (0%)	98,771 (1%)	104,318 (6%)
Mode 24	98,865	98,958 (0%)	117,339 (19%)	100,618 (2%)
Mode 25	100,889	100,948 (0%)	101,033 (0%)	111,100 (10%)

Note: % denotes the percentage difference compared to the CSRSM. N/A indicates that the mode cannot be obtained.

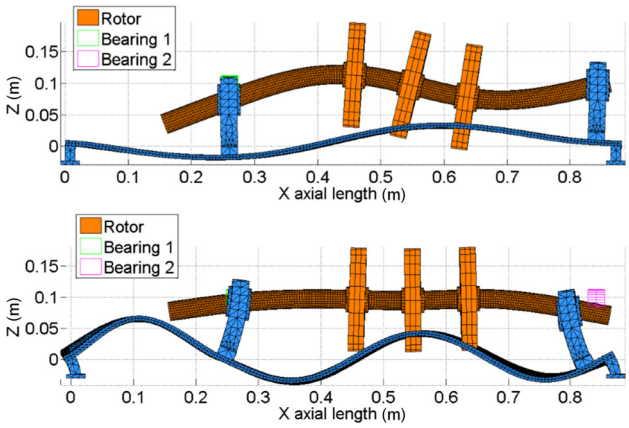

Fig. 20 Mode shapes of the solid FE rotor-support model corresponding to modes 7 (top) and 16 (bottom) in Table 2

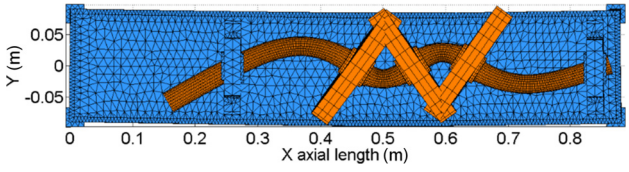

Fig. 21 Mode shape of the solid FE rotor-support model corresponding to mode 12 in Table 2

high-frequency support structure modes like mode 16 (bottom figure in Fig. 20), when the mode shape is more complicated. This can be remedied by dividing the support structure into more than one substructure. For example, the bearing pedestal could be separated as a substructure, or even the baseplate could be divided into several segments. However, the selection of substructures greatly depends on people's experience and may sacrifice the modeling time for accuracy.

With regard to the BRSSM, the prediction is fairly accurate (within 10% difference) for the lower-frequency modes but slightly inaccurate (10–20% difference) for the higher-frequency modes. This may be caused by the violation of the assumption in the beam theory that the plane sections remain plane after deformation. As can be observed from Fig. 21, the segments of the shaft between the disks are severely bending, which may result in the nonbeam deformation (i.e., the shaft sections are not plane after deformation).

From the comparison of the modes well above the operating speed range, it can be briefly concluded that the RSSM is more accurate than the SRSSM and BRSSM for the higher-frequency modes. Since the practical bandwidth of interest for AMB controllers is above 1000 Hz, the RSSM would be a good replacement of the SRSSM or BRSSM for the AMB-mounted turbomachinery. Moreover, the AMB controller can be easily integrated into the RSSM.

Summary and Conclusions

An improved rotordynamic modeling approach for a rotor-support system is proposed in the present paper. Instead of using the beam FEs, the rotor is modeled with the axisymmetric solid harmonic FEs, and the Guyan reduction method is applied to simplify the solid FE rotor model. The structure supporting the rotor can be represented by the TFs that are derived from the solid FE support model or measured FRFs of the substructure at the bearing locations. The way to find the curve fit for the FRFs of the support structure is also investigated. The frequency sampling and the polynomial degree of the TF are significant for the quality of curve-fitting. More specifically, a good excitation frequency sample should contain the response information in the neighborhood of the frequencies with a dramatic amplitude or phase change and should be the union of the frequencies of all the FRFs. In the meanwhile, the polynomial degree of the TF is better selected in such a way that the peaks and shifts of the TF amplitude or phase angle are retained by the curve fit with as a low polynomial degree as possible.

The TF matrix is further transformed into a state-space form and integrated into the rotor FE model. With the benefit of the

state-space form, controllers, actuators, and AMBs may be integrated in the rotor system.

To validate the proposed modeling approach, a thin-walled rotor with a flexible support is modeled using both the CSRSM and the RSSM. First, the RSSM is compared with the CSRSM. The comparisons made between natural frequencies, critical speeds, unbalance response, and log dec show that the RSSM provides a dynamically accurate approximation of the high-fidelity solid FE model. Furthermore, the comparison of the computation time shows that the proposed modeling approach is five times faster than the complete solid FE method in terms of the eigenvalue calculation. This time reduction factor may vary with the different number of DOFs of the rotor model and the support structure model.

Then, both the SRSSM and the BRSSM are included, together with the RSSM, in comparison of the modes up to 100,000 cpm (~1667 Hz) of the rotor system. The results confirm that the RSSM is more accurate in predicting the higher-frequency modes than the SRSSM and the BRSSM.

Acknowledgment

This research was supported by the Turbomachinery Research Consortium (TRC) at Texas A&M University.

Nomenclature

A_1, A_2 = attachment nodes of bearing 1 and 2
$[\mathbf{B}_{RB}]$, $[\mathbf{B}_{RU}]$ = matrices transforming bearing force and unbalanced force acted on the rotor from Cartesian coordinates into polar coordinates, respectively
BRSSM = beam FE rotor with a solid FE support model
CSRSM = complete solid FE rotor-support model
c, k = damping (N · s/m) and stiffness (N/m) coefficients of the bearing, respectively
DOF = degree-of-freedom
E = modulus of elasticity (N/m)
e = base of natural logarithm
F = external force (N)
F_{BY}, F_{BZ} = bearing forces in Y and Z direction, respectively (N)
FE = finite element
FRF = frequency response function
$\{\mathbf{f}\}$ = external load vector (N)
$\{\mathbf{f}_B\}$ = bearing force vector (N)
$\{\mathbf{f}_U\}$ = unbalanced force vector (N)
G_{AiBj} = frequency response function corresponding to the force acted on the bearing j in B direction and the response at the bearing i in A direction
$[\mathbf{G}_R]$ = gyroscopics matrix
$[\mathbf{G}(s)]$ = MIMO transfer function matrix
ith/jth = ith-order numerator divided by jth-order denominator
j = imaginary component
$[\mathbf{M}]$, $[\mathbf{C}]$, $[\mathbf{K}]$ = mass, damping, and stiffness matrices, respectively
MIMO = multiple-input and multiple-output
p-p = peak-to-peak
q = state variable
RSSM = reduced state-space model
SISO = single-input and single-output
SRSSM = solid FE rotor with a super-element support model
s = complex variable
TF = transfer function
U = displacements/DOFs (m)
u_r, u_z, u_θ = elemental displacements in the radial, axial, and tangential directions, respectively (m)
$\{\mathbf{y}\}$ = displacement vector in the Cartesian coordinates (m)
ρ = density (kg/m^3)
ν = Poisson's ratio
ω = excitation frequency of the unbalanced force (rad/s)
1/2/3-D = one/two/three-dimensional

Subscripts

B = bearing
$B1, B2$ = bearing 1 and 2
mS, mA = symmetric and antisymmetric components in mth harmonics, respectively
R = rotor
r, z, θ = radial, axial and circumferential directions, respectively
S = support structure
T = entire state-space model of the rotor-support system
U = unbalance
X, Y, Z = X, Y and Z directions in the Cartesian coordinates, respectively

Superscripts

A_1, A_2, B = nodes A_1, A_2, and B on the rotor, respectively
$\dot{}$ = derivative of time
$\hat{}$ = in the complex form

Appendix

The variables in the state-space model of the rotor and support are defined as follows:

$$\{\mathbf{q}_R\} = \begin{bmatrix} \{\dot{\mathbf{U}}_R\} \\ \hline \{\mathbf{U}_R\} \end{bmatrix} \tag{A1}$$

$$[\mathbf{A}_R] = \left[\begin{array}{c|c} -[\mathbf{M}_R]^{-1}[\mathbf{C}_R] & -[\mathbf{M}_R]^{-1}[\mathbf{K}_R] \\ \hline [\mathrm{I}] & [0] \end{array}\right] \tag{A2}$$

$$[\mathrm{B}_{RB}] = \begin{bmatrix} [\mathbf{M}_R]^{-1}[\mathrm{B}_{RB1}] \\ \hline [0] \end{bmatrix} \tag{A3}$$

$$[\mathrm{B}_{RB1}] = \begin{bmatrix} & \vdots & & \\ 1 & 1 & 0 & 0 \\ & \vdots & & \\ 0 & 0 & 1 & 1 \\ & \vdots & & \\ 1 & 0 & 0 & 0 \\ & \vdots & & \\ 0 & 0 & 1 & 0 \\ & \vdots & & \\ 0 & 1 & 0 & 0 \\ & \vdots & & \\ 0 & 0 & 0 & 1 \\ & \vdots & & \end{bmatrix} \text{ corresponding to } \begin{bmatrix} \vdots \\ U_{0rS}^{A_1} \\ \vdots \\ U_{0rS}^{A_2} \\ \vdots \\ U_{1rS}^{A_1} \\ \vdots \\ U_{1rS}^{A_2} \\ \vdots \\ U_{1rA}^{A_1} \\ \vdots \\ U_{1rA}^{A_2} \\ \vdots \end{bmatrix} \tag{A4}$$

$$\{\mathbf{f}_B\} = \begin{bmatrix} F_{BY1} \\ F_{BZ1} \\ F_{BY2} \\ F_{BZ2} \end{bmatrix} \tag{A5}$$

$$[\mathrm{B_{RU}}] = \begin{bmatrix} [\mathbf{M_R}]^{-1}[\mathrm{B_{RU1}}] \\ \hline [0] \end{bmatrix} \tag{A6}$$

$$[\mathrm{B_{RU1}}] = \begin{bmatrix} \vdots & \\ 1 & 1 \\ \vdots & \\ 1 & 0 \\ \vdots & \\ 0 & 1 \\ \vdots & \end{bmatrix} \text{ corresponding to } \begin{bmatrix} \vdots \\ U^B_{0rS} \\ \vdots \\ U^B_{1rS} \\ \vdots \\ U^B_{1rA} \\ \vdots \end{bmatrix} \tag{A7}$$

$$\{\mathbf{f_U}\} = \begin{bmatrix} F^B_{UX} \\ F^B_{UY} \end{bmatrix} \tag{A8}$$

$$[\mathbf{C_R}] = [\,[0] \,\vdots\, [\mathrm{C_{R2}}]\,] \tag{A9}$$

$$[\mathrm{C_{R2}}] = \begin{bmatrix} & \vdots & & \\ 1 & 1 & 0 & 0 \\ & \vdots & & \\ 0 & 0 & 1 & 1 \\ & \vdots & & \\ 1 & 0 & 0 & 0 \\ & \vdots & & \\ 0 & 0 & 1 & 0 \\ & \vdots & & \\ 0 & 1 & 0 & 0 \\ & \vdots & & \\ 0 & 0 & 0 & 1 \\ & \vdots & & \end{bmatrix}^T \text{ corresponding to } \begin{bmatrix} \vdots \\ U^{A_1}_{0rS} \\ \vdots \\ U^{A_2}_{0rS} \\ \vdots \\ U^{A_1}_{1rS} \\ \vdots \\ U^{A_2}_{1rS} \\ \vdots \\ U^{A_1}_{1rA} \\ \vdots \\ U^{A_2}_{1rA} \\ \vdots \end{bmatrix}^T \tag{A10}$$

In the state-space support model, $[\mathbf{A_S}]$, $[\mathrm{B_S}]$, and $[\mathbf{C_S}]$ are the minimal realization of the corresponding state-space matrices $[\tilde{\mathbf{A}}_\mathrm{S}]$, $[\tilde{\mathrm{B}}_\mathrm{S}]$, and $[\tilde{\mathbf{C}}_\mathrm{S}]$, which may be expressed as

$$[\tilde{\mathbf{A}}_\mathrm{S}] = \begin{bmatrix} [\mathbf{A}_{\mathrm{AiY1}}] & [0] & [0] & [0] \\ [0] & [\mathbf{A}_{\mathrm{AiZ1}}] & [0] & [0] \\ [0] & [0] & [\mathbf{A}_{\mathrm{AiY2}}] & [0] \\ [0] & [0] & [0] & [\mathbf{A}_{\mathrm{AiZ2}}] \end{bmatrix} \tag{A11}$$

$$[\mathbf{A}_{\mathrm{AiBj}}] = \begin{bmatrix} [\mathbf{A}_{\mathrm{Y1Bj}}] & [0] & [0] & [0] \\ [0] & [\mathbf{A}_{\mathrm{Z1Bj}}] & [0] & [0] \\ [0] & [0] & [\mathbf{A}_{\mathrm{Y2Bj}}] & [0] \\ [0] & [0] & [0] & [\mathbf{A}_{\mathrm{Z2Bj}}] \end{bmatrix} \tag{A12}$$

$$[\tilde{\mathrm{B}}_\mathrm{S}] = \begin{bmatrix} [\mathrm{B}_{\mathrm{AiY1}}] & [0] & [0] & [0] \\ [0] & [\mathrm{B}_{\mathrm{AiZ1}}] & [0] & [0] \\ [0] & [0] & [\mathrm{B}_{\mathrm{AiY2}}] & [0] \\ [0] & [0] & [0] & [\mathrm{B}_{\mathrm{AiZ2}}] \end{bmatrix} \tag{A13}$$

$$[\mathrm{B_{AiBj}}] = \begin{bmatrix} [\mathrm{B}_{\mathrm{Y1Bj}}] \\ [\mathrm{B}_{\mathrm{Z1Bj}}] \\ [\mathrm{B}_{\mathrm{Y2Bj}}] \\ [\mathrm{B}_{\mathrm{Z2Bj}}] \end{bmatrix} \tag{A14}$$

$$[\tilde{\mathbf{C}}_\mathrm{S}] = [\,[\mathbf{C}_{\mathrm{AiY1}}] \quad [\mathbf{C}_{\mathrm{AiZ1}}] \quad [\mathbf{C}_{\mathrm{AiY2}}] \quad [\mathbf{C}_{\mathrm{AiZ2}}]\,] \tag{A15}$$

$$[\mathbf{C}_{\mathrm{AiBj}}] = \begin{bmatrix} [\mathbf{C}_{\mathrm{Y1Bj}}] & [0] & [0] & [0] \\ [0] & [\mathbf{C}_{\mathrm{Z1Bj}}] & [0] & [0] \\ [0] & [0] & [\mathbf{C}_{\mathrm{Y2Bj}}] & [0] \\ [0] & [0] & [0] & [\mathbf{C}_{\mathrm{Z2Bj}}] \end{bmatrix} \tag{A16}$$

where the subscripts A, B indicate Y or Z, and $i, j = 1$ or 2. The entries of the state-space matrices shown in Eqs. (A12), (A14), and (A16) are derived from the TFs $G_{AiBk}(s)$ individually.

Suppose that there are two bearings involved (can be extended to any number), then the damping and stiffness matrices of the bearings are defined as

$$[\mathbf{C_B}] = \begin{bmatrix} c_{YY1} & c_{YZ1} & 0 & 0 \\ c_{ZY1} & c_{ZZ1} & 0 & 0 \\ 0 & 0 & c_{YY2} & c_{YZ2} \\ 0 & 0 & c_{ZY2} & c_{ZZ2} \end{bmatrix} \tag{A17}$$

$$[\mathbf{K_B}] = \begin{bmatrix} k_{YY1} & k_{YZ1} & 0 & 0 \\ k_{ZY1} & k_{ZZ1} & 0 & 0 \\ 0 & 0 & k_{YY2} & k_{YZ2} \\ 0 & 0 & k_{ZY2} & k_{ZZ2} \end{bmatrix} \tag{A18}$$

$$\{\mathbf{y_R}\} = \begin{bmatrix} U_{RY1} \\ U_{RZ1} \\ U_{RY2} \\ U_{RZ2} \end{bmatrix} \tag{A19}$$

$$\{\mathbf{y_S}\} = \begin{bmatrix} U_{SY1} \\ U_{SZ1} \\ U_{SY2} \\ U_{SZ2} \end{bmatrix} \tag{A20}$$

$$[\mathbf{A_T}] = \begin{bmatrix} [\mathrm{I}] + [\mathrm{B_{RB}}][\mathbf{C_B}][\mathbf{C_R}] & -[\mathrm{B_{RB}}][\mathbf{C_B}][\mathbf{C_S}] \\ -[\mathrm{B_S}][\mathbf{C_B}][\mathbf{C_R}] & [\mathrm{I}] + [\mathrm{B_S}][\mathbf{C_B}][\mathbf{C_S}] \end{bmatrix} \tag{A21}$$

$$[\mathrm{B_T}] = \begin{bmatrix} [\mathbf{A_R}] - [\mathrm{B_{RB}}][\mathbf{K_B}][\mathbf{C_R}] & [\mathrm{B_{RB}}][\mathbf{K_B}][\mathbf{C_S}] \\ [\mathrm{B_S}][\mathbf{K_B}][\mathbf{C_R}] & [\mathbf{A_S}] - [\mathrm{B_S}][\mathbf{K_B}][\mathbf{C_S}] \end{bmatrix} \tag{A22}$$

$$[\mathrm{B_{UT}}] = \begin{bmatrix} [\mathrm{B_{RU}}] \\ [0] \end{bmatrix} \tag{A23}$$

$$\{\mathbf{q}\} = \begin{bmatrix} \{\mathbf{q_R}\} \\ \{\mathbf{q_S}\} \end{bmatrix} \tag{A24}$$

where the state variable vector of the support structure $\{\mathbf{q_S}\}$ accompanies the generation of the matrices $[\mathbf{A_T}]$ and $[\mathrm{B_T}]$ and has no physical meanings.

References

[1] Nelson, H. D., and McVaugh, J. M., 1976, "The Dynamics of Rotor-Bearing Systems Using Finite Elements," ASME J. Eng. Ind., **98**(2), pp. 593–600.
[2] Nelson, H. D., 1980, "A Finite Rotating Shaft Element Using Timoshenko Beam Theory," ASME J. Mech. Des., **102**(4), pp. 793–803.
[3] Rouch, K. E., and Kao, J.-S., 1979, "A Tapered Beam Finite Element for Rotor Dynamics Analysis," J. Sound Vib., **66**(1), pp. 119–140.
[4] Greenhill, L. M., Bickford, W. B., and Nelson, H. D., 1985, "A Conical Beam Finite Element for Rotor Dynamics Analysis," ASME J. Vib., Acoust., Stress, Reliab., **107**(4), pp. 421–430.
[5] Vest, T. A., and Darlow, M. S., 1990, "A Modified Conical Beam Element Based on Finite Element Analysis: Experimental Correlations," ASME J. Vib. Acoust., **112**(3), pp. 350–354.
[6] American Petroleum Institute, 2002, "Axial and Centrifugal Compressors and Expander-compressors for Petroleum, Chemical and Gas Industry Services," API Publishing Services, Washington, DC, Standard No. API 617.
[7] Stephenson, R. W., Rouch, K. E., and Arora, R., 1989, "Modelling of Rotors With Axisymmetric Solid Harmonic Elements," J. Sound Vib., **131**(3), pp. 431–443.
[8] Stepheson, R. W., and Rouch, K. E., 1993, "Modeling Rotating Shafts Using Axisymmetric Solid Finite Elements With Matrix Reduction," ASME J. Vib. Acoust., **115**(4), pp. 484–489.
[9] Greenhill, L. M., and Lease, V. J., 2007, "Additional Investigations Into the Natural Frequencies and Critical Speeds of a Rotating, Flexible Shaft-Disk System," ASME Paper No. GT2007-28065.
[10] Cook, R. D., Malkus, D. S., Plesha, M. E., and Witt, R. J., 2001, *Concepts and Applications of Finite Element Analysis*, Wiley, New York.
[11] Stephenson, R. W., and Rouch, K. E., 1992, "Generating Matrices of the Foundation Structure of a Rotor System From Test Data," J. Sound Vib., **154**(3), pp. 467–484.
[12] Vázquez, J. A., and Barrett, L. E., 1999, "Transfer Function Representation of Flexible Supports and Casings of Rotating Machinery," 17th International Modal Analysis Conference, Kissimmee, FL, Feb. 8–11, pp. 1328–1334.

[13] Vaźquez, J. A., Barrett, L. E., and Flack, R. D., 2000, "A Flexible Rotor on Flexible Bearing Supports: Stability and Unbalance Response," ASME J. Vib. Acoust., **123**(2), pp. 137–144.
[14] Vaźquez, J. A., Barrett, L. E., and Flack, R. D., 2002, "Flexible Bearing Supports, Using Experimental Data," ASME J. Eng. Gas Turbines Power, **124**(2), pp. 369–374.
[15] Moore, J. J., Vannini, G., Camatti, M., and Bianchi, P., 2010, "Rotordynamic Analysis of a Large Industrial Turbocompressor Including Finite Element Substructure Modeling," ASME J. Eng. Gas Turbines Power, **132**(8), p. 082401.
[16] De Santiago, O., and Abraham, E., 2008, "Rotordynamic Analysis of a Power Turbine Including Support Flexibility Effects," ASME Paper No. GT2008-50900.
[17] Levy, E. C., 1959, "Complex-Curve Fitting," IRE Trans. Autom. Control, **AC-4**(1), pp. 37–43.
[18] Franklin, G. F., Powell, J. D., and Emami-Naeini, A., 2005, *Feedback Control of Dynamic Systems*, Prentice-Hall, Upper Saddle River, NJ.
[19] Guyan, R. J., 1965, "Reduction of Stiffness and Mass Matrices," AIAA J., **3**(2), p. 380.
[20] Rosenbrock, H. H., 1970, *State-Space and Multivariable Theory*, Wiley, New York.
[21] Pace, I. S., and Barnett, S., 1974, "Efficient Algorithms for Linear System Calculations—Part II Minimal Realization," Int. J. Syst. Sci., **5**(5), pp. 413–424.
[22] Van Dooren, P., 1981, "The Generalized Eigenstructure Problem in Linear System Theory," IEEE Trans. Autom. Control, **26**(1), pp. 111–129.